RESEARCH ARTICLE

VOLCANICA

A shake and a surge: Assessing the possibility of an earthquake-triggered eruption at Steamboat Geyser

Mara H. Reed*[α], Anna Barth[α], Taka'aki Taira[β], Jamie Farrell[γ], and Michael Manga[α,β]

[α] Department of Earth and Planetary Science, University of California, Berkeley, Berkeley, USA.
[β] Berkeley Seismological Lab, University of California, Berkeley, Berkeley, USA.
[γ] Department of Geology and Geophysics, University of Utah, Salt Lake City, USA.

Abstract

When and why earthquakes trigger volcano and geyser eruptions remains unclear. In September 2022, Steamboat Geyser in Yellowstone, USA erupted 8.25 hours after a local M3.9 earthquake—an improbable coincidence based on the geyser's eruption intervals. We leverage monitoring data from the surrounding geyser basin to determine if the earthquake triggered this eruption. We calculate a peak ground velocity of 1.2 cm s^{-1}, which is the largest ground motion in the area since Steamboat reactivated in March 2018 and exceeds a threshold associated with past earthquake-triggered geyser eruptions in Yellowstone. Despite no changes in other surface hydrothermal activity, we found abrupt, short-lived shifts in ambient seismic noise amplitude and relative seismic velocity in narrow frequency bands related to the subsurface hydrothermal system. Our analysis indicates that Steamboat's eruption was likely earthquake-triggered. The hours-long delay suggests that dynamic strains from seismic waves altered subsurface permeability and flow which enabled eruption.

Keywords: Geyser; Hydrothermal; Eruption triggering; Dynamic stress.

Submitted: 2024-01-03 | Accepted: 2024-08-08 | Published: 2024-10-17

Editor: O. Lamb | Typesetter: C. Harnett

1 Introduction

Stress changes produced by earthquakes affect the properties and flow of fluids in the crust. Earthquakes can promote the eruption of magmatic volcanoes [e.g. Linde and Sacks 1998; Walter et al. 2007; De la Cruz-Reyna et al. 2010; Bebbington and Marzocchi 2011] and mud volcanoes [e.g. Mellors et al. 2007; Bonini et al. 2016; Zhong et al. 2019], change the interval between geyser eruptions [Husen et al. 2004; Hurwitz et al. 2014], and modify the composition, pressure, and flow of groundwater [Wang and Manga 2021]. The roles of static and dynamic stresses, as well as the physical properties and processes that change, remain the subject of active research [Seropian et al. 2021].

Modifications to volcanic unrest may become apparent in the minutes to days following an earthquake [e.g. Walter et al. 2007], but volcanic eruptions are most likely triggered within months to years [Walter and Amelung 2007; Nishimura 2017; Sawi and Manga 2018]. However, confidently linking volcanic eruptions to specific earthquakes is statistically fraught since eruptions occur so infrequently [Sawi and Manga 2018; Seropian et al. 2021]. In the case of geysers, which are often billed as more active and accessible analogs for volcanoes [Kieffer 1984; Hurwitz et al. 2021], frequent eruptions and faster earthquake response times mitigate this problem. Changes to surface activity at geyser fields after large regional earthquakes near Yellowstone, USA [Marler and White 1975; Hutchinson 1985] and Haukadalur, Iceland [Thorkelsson 1940; Barth 1950; Pálmason 2002] are historically well documented. Geysers can also be affected by teleseismic events, such as altered eruptive activity in Yellowstone's Upper Geyser Basin following the 3100 km distant 2002 M7.9 Denali earthquake [Husen et al. 2004].

Hurwitz et al. [2014] found that seismic waves must create dynamic stresses on the order of 10^{-1} MPa to affect geysers based on the responses and non-responses of Old Faithful and Daisy Geysers to 21 teleseismic earthquakes. The lack of known earthquake-triggered geyser eruptions following small, local earthquakes may suggest that geysers are more sensitive to long period seismic waves and/or longer shaking duration. This sensitivity is observed in other pressurized systems, including for example eruptive flow rates at the Davis-Shrimpf mud volcanoes [Rudolph and Manga 2012] and triggered seismicity at Long Valley Caldera [Brodsky and Prejean 2005], both in the USA. Unfortunately, most geyser monitoring is discontinuous with data that are not robust enough to distinguish short-lived changes to eruptive activity, so it is possible small earthquake triggers have simply escaped scientific inquiry due to a lack of data.

We present a candidate earthquake-triggered eruption of a geyser following a small earthquake where, crucially, seismic data were available. Steamboat Geyser at Norris Geyser Basin in Yellowstone National Park, USA has powerful major eruptions that reach heights in excess of 120 m. Most eruptions occur during active phases that last for months to years and are separated by periods of quiescence that last for years to decades [Reed et al. 2021]. The most recent active phase began on 15 March 2018 and as of early October 2024, there have been 173 major eruptions, the greatest number of eruptions in any known active phase. On 18 September 2022, Steamboat erupted after an interval of 90 days, the longest time between eruptions during the active phase thus far. The eruption began 8.25 hours after a M_L 3.9 earthquake with an epicenter 11 km from the geyser [University of Utah Seismograph Stations 2022].

This paper is structured to emphasize the investigative process we followed to determine whether earthquake-triggering

* mhreed@berkeley.edu

was plausible. We first summarize the relevant monitoring data from Norris Geyser Basin. Then, we estimate the probability of Steamboat erupting on 18 September by chance and determine whether that eruption's properties were similar or different to other eruptions in the ongoing active phase. Next, we describe the M3.9 earthquake and calculate the peak ground velocity associated with it and other earthquakes since 2018. We search for any response in the hydrothermal system beyond Steamboat by analyzing activity at Whirligig Geyser, the only other active geyser at that time for which eruptions can be discerned from the available data, and checking for fluctuations in the total thermal water outflow from Norris Geyser Basin. Finally, we investigate changes in ambient seismic noise and relative seismic velocity related to the subsurface hydrothermal system. The last two sections are reserved for a discussion of this event in the context of other triggered eruptions and a summary of our findings.

2 Available data

Norris Geyser Basin (Figure 1), also known simply as Norris, is well-monitored by sensors compared to other thermal areas in Yellowstone. The University of Utah operates the Yellowstone Seismic Network (code WY) which provides a 1.5 magnitude of completeness [Farrell et al. 2009]. Relevant to this study are two broadband stations located in the Norris area with Nanometrics Trillium instruments sampling at 100 Hz. Station YNM (long period corner 240 s) is situated in a shed within the geyser basin 340 m to the north of Steamboat while station YNR (long period corner 120 s) is located 2.19 km to the southeast. Both stations record significant anthropogenic noise during daylight hours. Their data are hosted in the EarthScope Consortium Data Management Center*.

In addition to the seismometers, there is a U.S. Geological Survey streamgage that measures flow on Tantalus Creek every 15 minutes†. Tantalus Creek is a thermal stream that captures nearly all discharge from geysers and hot springs at Norris [Friedman 2007]. The geyser basin also hosts a small network of sensors that record temperatures every two minutes at select hot springs and geysers [Yellowstone Volcano Observatory 2023]. When placed in runoff channels, temperature sensors can record eruptions (sudden spikes in temperature) and provide information about relative thermal outflow (higher temperatures indicate increased flow through the channel). The clocks within the temperature sensors do not sync to GPS and drift over time, though this can be corrected for sensors at geysers given sufficient visual observations. Raw temperature data used in this study can be found in Supplementary Material 1.

Major eruptions of Steamboat Geyser are detectable at a temperature sensor placed in one of Steamboat's runoff channels, the Tantalus Creek streamgage, and both the YNM and YNR seismic stations. Because its eruptions are so spectacular, Steamboat is also tracked closely by geyser enthusiasts who submit eruption data and visual observations to the crowdsourced database GeyserTimes. A complete catalog of Steamboat eruptions exists for the recent active phase. Visual observations for most other Norris geysers are too sporadic to ascertain any subtle changes resulting from the M3.9 earthquake. Whirligig and Constant Geysers, a pair of pool geysers ~580 m north of Steamboat, are the only other active geysers at Norris in 2022 that were monitored by a temperature sensor. Most eruptions of Whirligig are recorded but the temperature sampling frequency is too low to record eruptions of Constant.

*https://ds.iris.edu/ds/nodes/dmc/

†https://waterdata.usgs.gov/monitoring-location/06036940

3 The case for a triggered eruption of Steamboat Geyser

When geysers have regular eruption intervals, identifying perturbations by earthquakes and other external influences is straightforward [Rinehart 1974; Husen et al. 2004; Hurwitz et al. 2014]. Steamboat's eruptions were somewhat regular during 2018–2020 when there was a small seasonal modulation of eruption intervals correlated with the hydrological cycle [Reed et al. 2021] and the average interval was 8 days. However, intervals became more erratic over time (Figure 2A) and the average interval was 26 days for eruptions in 2021 through August 2023. To investigate whether earthquake triggering of the 18 September 2022 eruption is plausible, we quantify the probability of Steamboat erupting on that day regardless of whether there was an earthquake and check whether any aspect of the eruption was atypical. We also calculate the peak ground velocity generated at Norris Geyser Basin from the M3.9 earthquake and determine whether it or any other earthquakes since 2018 exceeded the 0.1 MPa dynamic stress threshold for geyser response determined by Hurwitz et al. [2014].

3.1 Probability analysis

What is the probability that the eruption coincidentally occurred after the earthquake? To obtain a simple estimate of how likely Steamboat was to erupt on 18 September 2022, we divide the number of days on which eruptions occurred (156) by the number of days in the active phase up to but not including 18 September 2022 (1648). This method yields a probability of 9.5 % but does not take the geyser's changing eruption intervals into account, nor that the post-earthquake eruption occurred after an unusually long interval.

An alternative approach is to model the probability distribution of Steamboat's eruption intervals and then calculate the conditional probability of an interval that would place the eruption in a short time window after the earthquake. For the model, we fit a Fréchet distribution to the population of eruption intervals before the candidate earthquake-triggered eruption (Figure 2B). The three-parameter Fréchet distribution is a strongly right-skewed extreme value distribution with a cumulative distribution function defined as

$$\mathrm{CDF}_{\text{Fréchet}}(x) = e^{-\left(\frac{x-m}{\beta}\right)^{-\alpha}} \tag{1}$$

for $x > m$ and where α, β, and m are the shape, scale, and location parameters. We fix $m = 0$ and use the method of maximum likelihood estimation to fit the shape and scale parameters.

Next, we define two probabilities related to the time between the last Steamboat eruption and the M3.9 earthquake

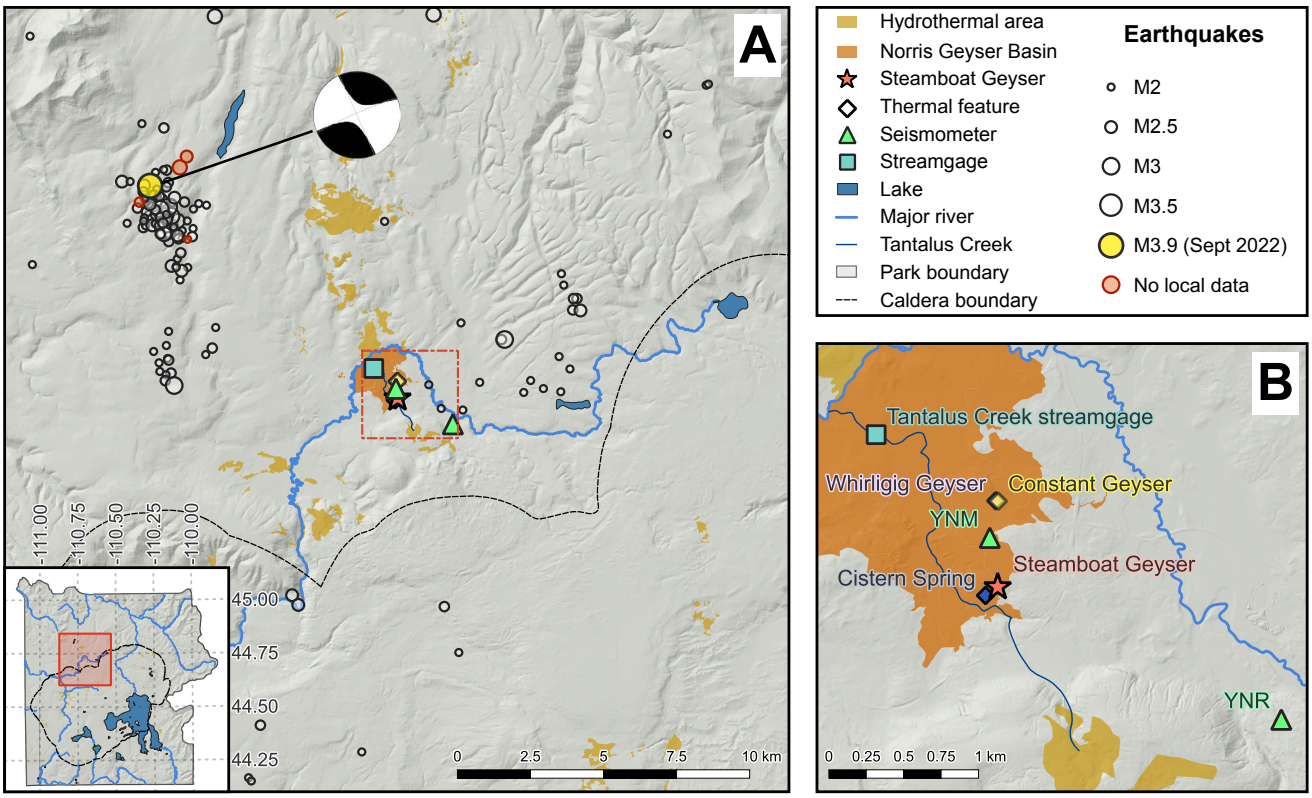

Figure 1: [A] Locations of local ≥ M2 earthquakes occurring in March 2018 through August 2023 in our search area. The M3.9 earthquake is marked in yellow and labeled with the focal mechanism determined by University of Utah Seismograph Stations [2022]. Red circles show the 4 local earthquakes for which both YNM and YNR were offline. The extent of [A] corresponds to the red box on the inset map. [B] Locations of thermal features and monitoring equipment within and near Norris Geyser Basin. Whirligig and Constant Geysers are located ~15 m apart. The extent of [B] corresponds to the red dashed box in [A].

(89.6 days). Let $P(A)$ represent the probability that Steamboat has an eruption interval of ≤90.6 days and $P(B)$ represent the probability that Steamboat has an interval >89.6 days. In other words, $P(A)$ is the chance of Steamboat erupting at any point up to 24 hours after the earthquake whereas $P(B)$ is the chance that Steamboat has not erupted before the earthquake. We obtain these probabilities by using our Fréchet model:

$$P(A) = \mathrm{CDF}_{\mathrm{Fréchet}}(90.6) \simeq 9.985 \times 10^{-1}; \quad (2)$$

$$P(B) = 1 - \mathrm{CDF}_{\mathrm{Fréchet}}(89.6) \simeq 1.587 \times 10^{-3}. \quad (3)$$

Then, we use Bayes' theorem to evaluate the conditional probability that Steamboat has an interval of ≤90.6 days given that it has been 89.6 days without an eruption:

$$P(A|B) = P(B|A) \times \frac{P(A)}{P(B)} = \frac{P(A) - (1 - P(B))}{P(A)} \times \frac{P(A)}{P(B)} = \frac{P(A) - (1 - P(B))}{P(B)}. \quad (4)$$

Substituting our values from Equation 2 and 3 into Equation 4, we find that the probability of Steamboat erupting within 24 hours after the earthquake is 2.7 %.

3.2 Eruption properties

Was the 18 September 2022 eruption unusual in any way? Typical major eruptions at Steamboat start with a <2-hour long water jetting phase that builds to a maximum height of 85–137 m [Vander Ley 2021] in the first few minutes and then subsides to heights below 60 m. Following this, the jet becomes more steam-dominated (Figure 3). The eruption may later transition multiple times between water and steam phases until finally entering a low-energy steam phase that tapers to quiescence. The full eruption duration including all water and steam phases typically lasts several hours to a few days. Following each major eruption, the nearby Cistern Spring will drain and then refill over several days [White et al. 1988; Wu et al. 2021]. Comparatively small minor eruptions reaching <15 m occur frequently between major eruptions.

Following the earthquake at 6:55 local time (UTC-6) on 18 September, there was no change to flow down Steamboat's south runoff channel as inferred from temperature data (Figure 4A) and an in-basin observer reported "nothing abnormal" when checking on the geyser at 7:16 [Wolf 2022]. Later, a different observer in the vicinity of Norris Geyser Basin heard the major eruption begin at 15:10 and reported an initial water phase duration of 10 minutes [Beverly 2022]. We determine the volume of the water discharge pulse (Figure 4B) from the eruption by manually picking the start and end times, inter-

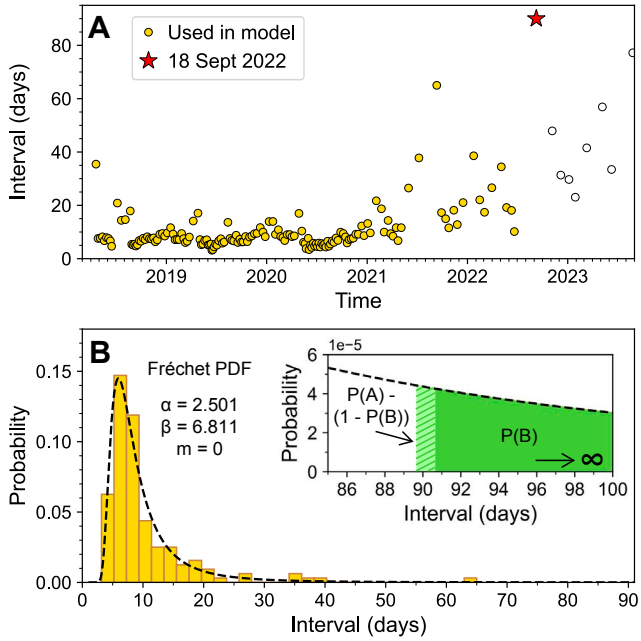

Figure 2: [A] Interval between Steamboat's eruptions over time. [B] Probability density function for the Fréchet fit (black dashed line) overlaid on probabilities for the real interval population before the 18 September 2022 eruption. The inset panel visualizes the numerator (light green shading) and the denominator (dark green shading, including the hatched area) from the result of Equation 4, which represents the probability of Steamboat erupting within 24 hours of the earthquake given that the geyser had not already erupted. Note that we show the probability density function here rather than the cumulative density function. Evaluating the cumulative density function at any given interval is equivalent to integrating the probability density function up to that interval.

polating baseflow, and subtracting baseflow volume from the total volume. This yields a volume of 373 m^3; however, wind speeds >1 m s^{-1} decrease the water volume that enters Tantalus Creek and thus this should be considered a minimum estimate [Reed et al. 2021]. In terms of both vertical seismic velocity spectral content (Figure 4C) and ejected water volume, the 18 September eruption was similar to other major eruptions [Reed et al. 2021; Reed and Manga 2023]. Cistern Spring also drained and refilled as normal. The only unusual aspect of this eruption was its long full duration of ~4 days. However, this is likely related to the 90-day eruption interval rather than the earthquake, given that a different lengthy interval of 77.2 days also resulted in an eruption with a long full duration of >3.6 days [Beverly 2023].

3.3 Peak ground velocity comparison

Did the M3.9 earthquake generate enough stress to affect a geyser? This event was the largest in the Grizzly Lake sequence, an intermittently active swarm that began in January 2022 and by the end of the year accumulated 1,177 events, >500 of which occurred during September [Yellowstone Volcano Observatory 2023]. Swarms are sequences of earthquakes clustered in space and time that do not have a well-defined mainshock [Mogi 1963]. In Yellowstone, they have been attributed to magmatic and hydrothermal fluid migration [Waite and Smith 2002; Farrell et al. 2010; Shelly et al. 2013], and as many as half of all earthquakes in the Yellowstone area occur as part of swarms [Farrell et al. 2009].

The 0.1 MPa dynamic stress threshold for earthquake-triggered effects at the geysers studied by Hurwitz et al. [2014] corresponds to a peak ground velocity (PGV) of 1 cm s^{-1}. To obtain the PGV at Norris Geyser Basin due to the M3.9 earthquake, we download three-component seismic data for station YNM from the EarthScope Consortium Data Management Center, demean the data, and remove the instrument response to obtain velocity records. Because YNM is a noisy station located by a popular trail, we apply a 4th-order, acausal Butterworth bandpass filter between 0.8 and 30 Hz to reduce contributions from high-frequency anthropogenic and low-frequency ambient noise. We calculate the magnitude of 3D ground motion and find a PGV of 1.2 cm s^{-1}.

The next step is to put this PGV in context with ground motions produced by other earthquakes since Steamboat's recent active phase began. For the period of March 2018 through August 2023, we search the Advanced National Seismic System (ANSS) Comprehensive Catalog and identify 135 local earthquakes ≥M2 in a rectangular area bounded by latitudes (44.603, 44.843) and longitudes (-110.873, -110.533) (Figure 1A), 12 regional earthquakes ≥M5 within a 1000 km radius of Steamboat, and 751 teleseismic earthquakes ≥M6. At least one or both of stations YNM and YNR was operating for 131 (97.0 %) of the local earthquakes, all 12 of the regional earthquakes, and 711 (94.7 %) of the teleseismic earthquakes. Most of the missed events occurred when YNM and YNR were both offline in January through April 2023, but it is unlikely that our analysis excludes any significant events. None of the missed local earthquakes during this period exceeded M2.9 and none of the missed ≥M7 teleseismic earthquakes occurred within 5700 km.

We calculate PGV at both YNM and YNR for the local earthquakes by following the same procedure as before. For the regional and teleseismic earthquakes, we use the same procedure but filter between 0.05 and 10 Hz to capture long period seismic arrivals. Instrument response correction can sometimes amplify unwanted noise at low frequencies [Havskov and Alguacil 2016], so we use the comparatively less noisy YNR data to ground truth the YNM values. There is significant (>1 order of magnitude) PGV disparity for 30 teleseismic events which we manually reviewed and confirmed noise contamination at YNM.

Figure 5 shows the 119 local, 3 regional, and 47 teleseismic earthquakes exceeding a PGV of 10^{-2} cm s^{-1}. Values at YNM are shown unless that station was offline or noisy, in which case we substituted the PGV at YNR. The M3.9 earthquake produced the greatest PGV experienced at Norris Geyser Basin during Steamboat's recent active phase and is the only event to exceed 1 cm s^{-1}. The next highest PGV of 0.8 cm s^{-1} is associated with a M7.6 earthquake in southwestern Mexico that occurred just one day later on 19 September. Of the next three highest PGV events, only the M6.5 Stanley,

Figure 3: Steamboat Geyser in steam phase on 18 September 2022 at 17:58 local time (2.8 hours after eruption initiation). Photo by Graham Meech.

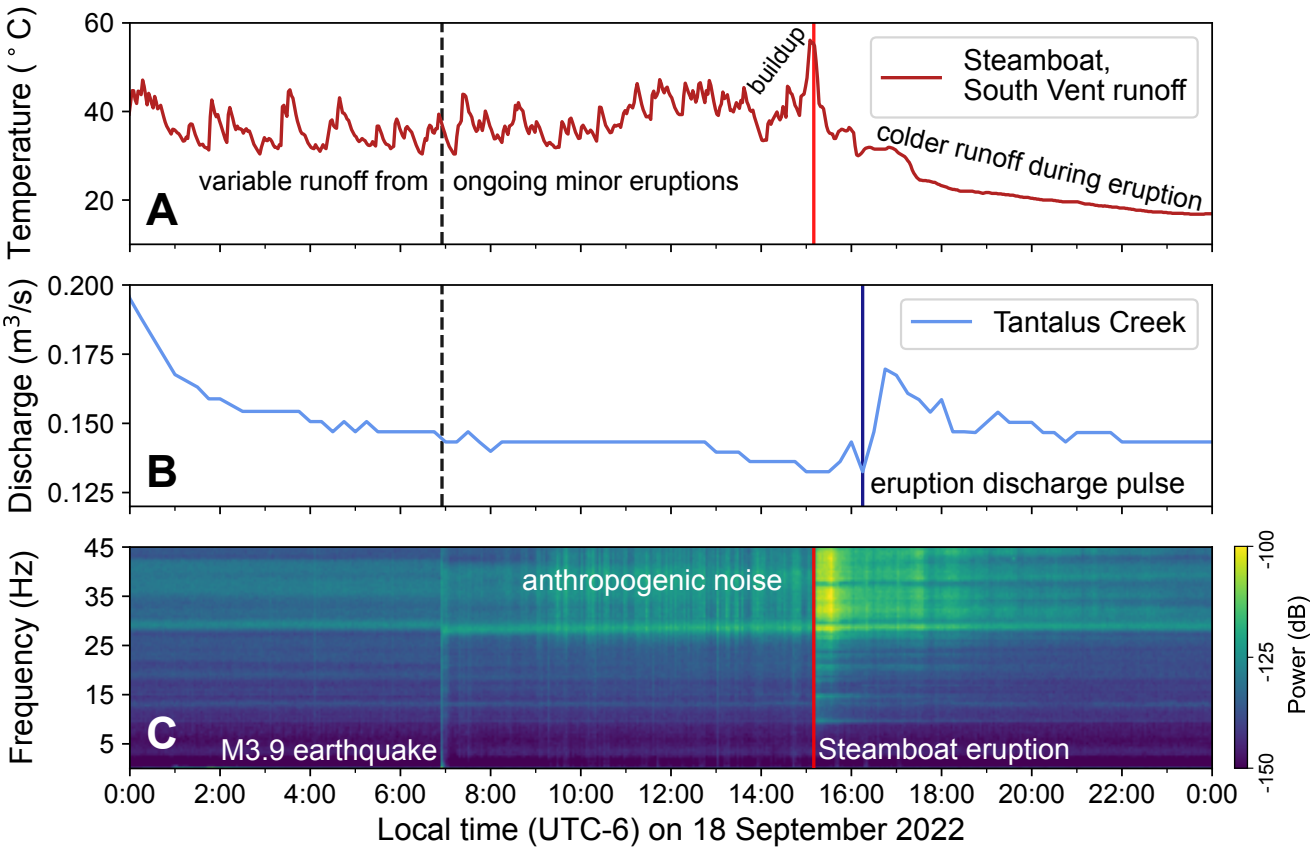

Figure 4: A visual summary of Steamboat eruption signals on 18 September 2022. [A] Temperature data from Steamboat's South Vent runoff channel. The temperature drops during the eruption because water discharges through the jet and cools while traveling through the air. [B] Hot spring and geyser discharge through Tantalus Creek. The pulse from Steamboat's eruption is delayed because erupted water travels over 2 km through Tantalus Creek before reaching the streamgage. [C] Spectrogram of YNM vertical velocity; power is clipped to the upper (-100 dB) and lower (-150 dB) bounds. The spectrogram was computed from vertical component data that was corrected for instrument response. In panels [A] and [B], the earthquake timing is marked with a black dashed line. In panels [A] and [C], Steamboat's eruption start time is shown with a red line.

Idaho earthquake with a PGV of 0.5 cm s^{-1} occurred within close proximity (33.8 hours prior) to a Steamboat eruption, but the 8.3-day interval before this eruption was not anomalously short.

4 The case for other hydrothermal changes

So far, we have established the low probability that Steamboat erupted on the same day as the M3.9 earthquake by coincidence, that the PGV associated with this earthquake is above a threshold known to impact other Yellowstone geysers, and that this PGV was the largest recorded at Norris Geyser Basin since the ongoing active phase began in March 2018. We now search for any evidence that the M3.9 earthquake affected surface activity at other geysers in Norris or changed the subsurface hydrothermal system.

4.1 Surface hydrothermal activity

Did other monitored thermal features at Norris Geyser Basin react to the earthquake? Visual observers did not report any striking changes such as increased turbidity or signs of unusual eruptive activity at thermal features that can be seen from trails. Since there were no anomalous signals in the Tantalus Creek streamflow data other than the pulse from Steamboat's eruption (Figure 4B), we can also infer there was no significant change in total discharge from thermal features at Norris on 18 September 2022. Though continuous monitoring of specific thermal features is limited, we can assess the earthquake's impact on Whirligig Geyser, a small geyser 580 m north of Steamboat for which we have runoff channel temperature data. There are two types of Whirligig eruptions that are historically classified as eruptions and minor eruptions. We will refer to the former as major eruptions for clarity. Major eruptions discharge water out of three vents for several minutes and conclude when the pool almost fully drains; the shorter minor eruptions are accompanied by lethargic splashing and end with a small drop in pool water level. All major eruptions are detected when the sensor is operating but minor eruptions can be missed when they last less than a minute or begin from a pool level below overflow. Additionally, the runoff channel where the temperature sensor is placed receives variable outflow from Constant Geyser and a weak minor eruption signal from Whirligig can be overprinted during peak discharge from Constant.

We show temperature data recorded on 18 September 2022 in Figure 6. Timestamps are shifted forward by six minutes, which is the estimated sensor clock offset based on visual observations of eruptions recorded in GeyserTimes. Major eruptions at Whirligig can be seen as large temperature spikes reaching >60 °C while minor eruptions correspond to the much smaller temperature spikes. The temperature oscillation with a period of 20–30 minutes is due to a cycling water level in Constant Geyser which affects outflow volume and thus temperature recorded in the channel. In the hours following the earthquake, there was no change to discharge cycling at Constant nor eruption intervals at Whirligig. The only possible indication of a reaction at Whirligig is the small temperature increase nearly concurrent with the earthquake (Figure 6 inset). While not marked in the GeyserTimes database as an eruption, this signal bears similarities to minor eruptions confirmed by in-basin observers but not clearly reflected in the temperature data (gold dotted lines between 12:00 and 14:00 in Figure 6). If this was indeed a minor eruption, the preceding 47-minute interval is notable because major-to-minor intervals of <60 minutes are uncommon. However, due to the uncertainty in the logger clock offset and the challenges of discerning minor eruptions in the shared runoff channel, we cannot confirm that this minor eruption took place nor that it began after the earthquake.

There remains the possibility for delayed or gradual changes to Whirligig Geyser and discharge through Tantalus Creek, so we also explore data from August through October 2022 to assess long-term trends (Figure 7). We use eruptions in the GeyserTimes catalog to calculate three different measures of Whirligig's activity. Due to the sensor clock issue, we only use GeyserTimes entries with an electronic (E) timecode for calculating intervals, meaning the eruption start time was derived from temperature data. First, we separate the data into daily slices and determine both the mean interval prior to detected eruptions and the fraction of minor eruptions for each day (Figure 7A). Because some minor eruptions go undetected, the mean interval is likely overestimated and the fraction of minor eruptions is underestimated. We finally calculate major-to-major eruption intervals (Figure 7B). We present Tantalus Creek discharge as both raw data and after applying an acausal, 2nd order Butterworth lowpass filter to remove periods shorter than 2 days (Figure 7C).

Over this three-month period, the daily fraction of minor eruptions at Whirligig increased to reach >0.85 in all of October. The daily mean interval became less variable between mid-September and 10 October before returning to the same length and variability seen in August. Major-to-major intervals generally increased through September, becoming more variable in mid-September with a steeper increasing trend that continued through October. None of these changes appear tied to the M3.9 earthquake on 18 September.

The Tantalus Creek hydrograph shows a slight upward trend through the selected time period which does not change following the earthquake. At shorter timescales, there were sharp discharge peaks associated with rainfall events except for the spike on 18 September which is caused by runoff from Steamboat's eruption (Figure 4B). There was a small drop in discharge through 19 September, but such variations are common through this time period. Thus, we again find no support for an earthquake response in the overall thermal discharge from Norris.

4.2 Subsurface hydrothermal tremor

Were there any changes to the strength of ambient seismic noise? Hydrothermal areas generate tremor that has been primarily attributed to bubble collapse and occasionally bubble nucleation [e.g. Kedar et al. 1998; Legaz et al. 2009; Cros et al. 2011; Vandemeulebrouck et al. 2014; Wu et al. 2017; Nayak et al. 2020; Eibl et al. 2021]. Very little has been published about hydrothermal tremor at Norris Geyser Basin since Iyer and Hitchcock [1974] identified the area as a source of seismic noise. Dawson et al. [2012] detected localized, >15 Hz im-

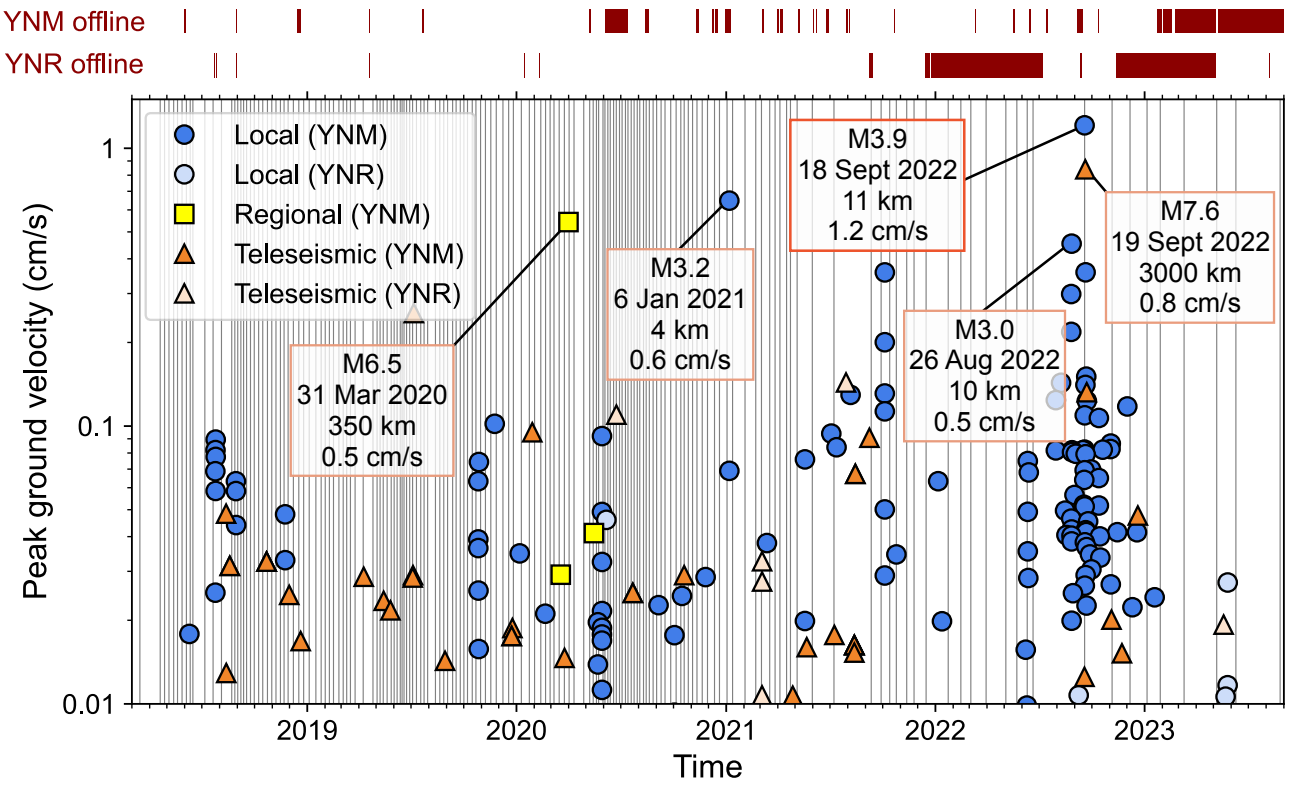

Figure 5: PGV associated with local, regional (<1000 km), and teleseismic earthquakes between March 2018 and September 2023. YNR values (lighter colors) are shown when YNM was offline or noisy. Grey vertical lines mark Steamboat eruptions and dark red boxes above the plot show data gaps for the two broadband stations. We label five events associated with the greatest PGVs including the M3.9 earthquake (red box) with their magnitude, date, distance from Steamboat, and PGV.

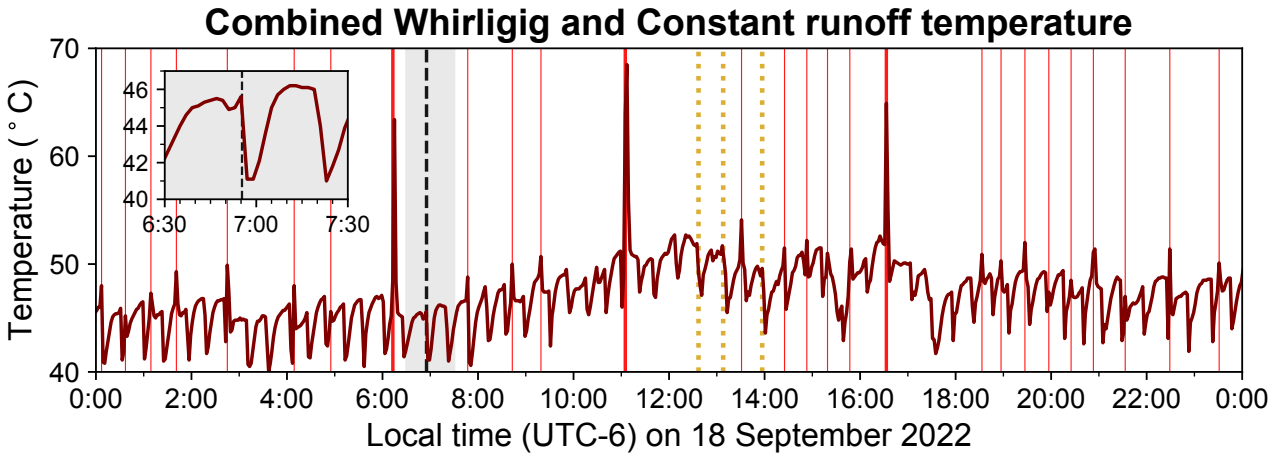

Figure 6: Temperature data from a runoff channel which receives discharge from Whirligig and Constant Geysers. The M3.9 earthquake is marked by a black dashed line. Solid red lines mark major (thick lines) and minor eruptions (thin lines) with an electronic (E) timecode in the GeyserTimes database. Gold dotted lines indicate visually confirmed minor eruptions that did not have corresponding E timecode entries in GeyserTimes, illustrating how minor eruptions do not always produce clear temperature signals. Short period temperature oscillations are due to cycling discharge from Constant Geyser. The inset panel is a zoomed-in view of the time period marked by the grey box which shows a small temperature peak that could indicate a minor eruption.

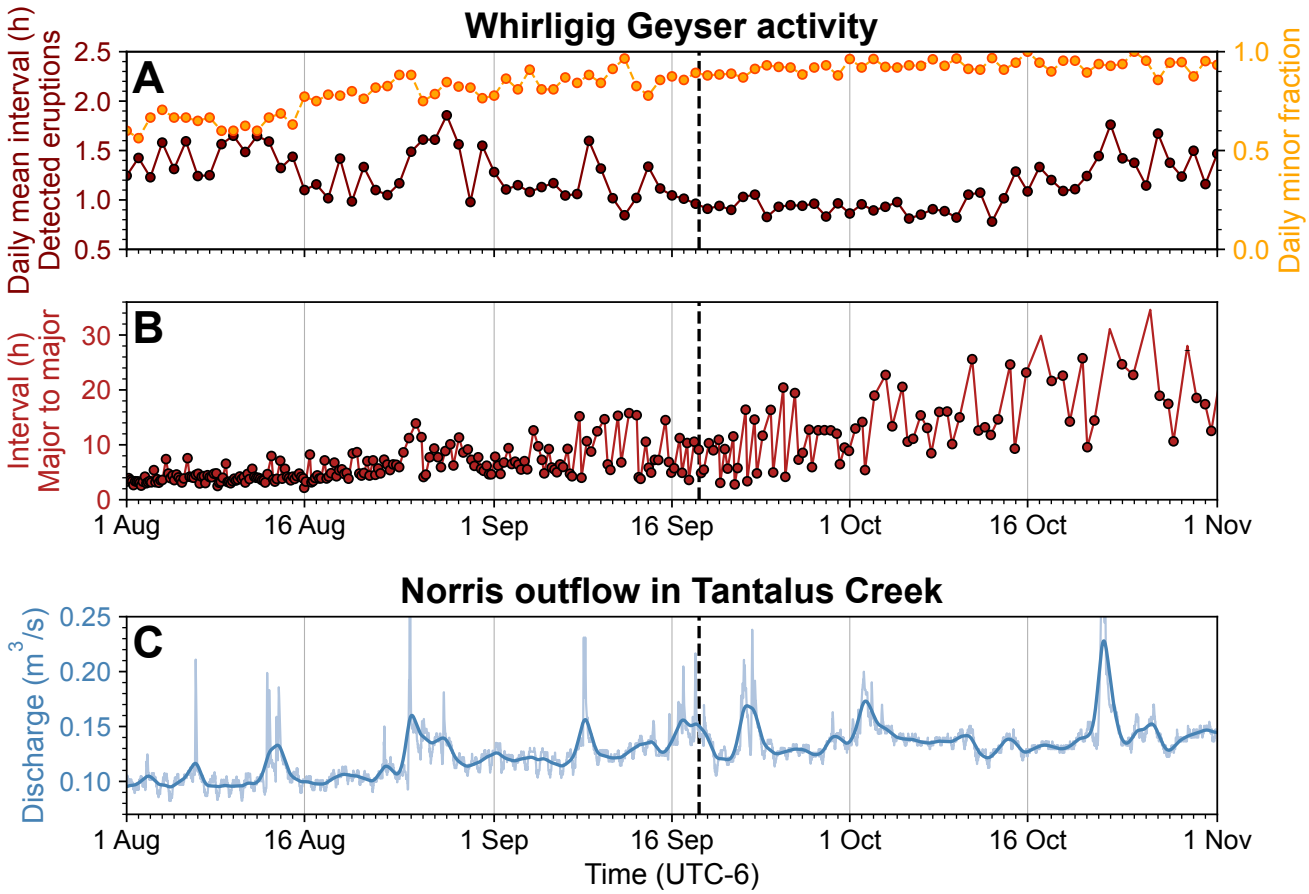

Figure 7: Measures of Whirligig Geyser activity and total thermal water outflow from Norris Geyser Basin. The black dashed line in each panel marks the time of the M3.9 earthquake. [A] Daily mean interval for Whirligig Geyser eruptions detected in temperature data (dark red). We also show the fraction of minor eruptions occurring each day (orange). [B] Intervals between major eruptions at Whirligig. [C] Raw discharge in Tantalus Creek (light blue) and the result of applying a 2-day lowpass filter (dark blue). All discharge spikes occur due to rainfall events except for the pulse from Steamboat's eruption on 18 September.

pulses occurring 1–2 times per second and continuous 8 Hz tremor in the southern half of Norris Geyser Basin during a 2003 broadband seismometer campaign. Wu et al. [2021] deployed a dense nodal array around Steamboat Geyser and Cistern Spring and found continuous 1–5 Hz tremor that varied in space and amplitude over Steamboat's eruptive cycle. While station YNM is likely too far away to detect tremor sources local to Steamboat when the geyser is not erupting, we can still explore the relative power of any hydrothermal tremor local to the station.

Seismic spectral amplitude measurements (SSAM) are a computationally inexpensive way to represent relative signal strength in different frequency bands over time [Rogers and Stephens 1995]. We compute SSAM for narrow 1 Hz bands between 0.5 to 5.5 Hz, a range chosen to match low frequency tremor observed in Yellowstone thermal areas [Wu et al. 2019; 2021; Liu et al. 2023] and to avoid contamination from Steamboat's broadband (5–45 Hz) eruption signal [Reed and Manga 2023]. After selecting the raw, vertical-component seismic data for overnight hours (20:30–6:30 local time) during August–October 2022, we remove instrument response to obtain velocity, slice the data into 1-hour segments, and apply acausal, 4th order Butterworth bandpass filters to match the bands of interest. We then calculate SSAM as the median of the absolute valued velocity in each segment.

Only the 0.5–1.5 Hz SSAM show a response to the earthquake (Supplementary Material 2 Figure S1). In this band, SSAM gradually increase over the long term from 18 to 22 nm s^{-1} up until the M3.9 earthquake, after which there is a 3 nm s^{-1} downward step change (Figure 8A). The long-term trend is punctuated by SSAM peaks that occur every 10–12 days and correlate with a cyclic reduction in minor eruptive activity at Steamboat Geyser as inferred from temperature data (Supplementary Material 2 Figure S2), suggesting a common process that affects both Steamboat and the source of this SSAM signal. The 10–12 day period does not change following the earthquake. We compute spectrograms of the unfiltered vertical seismic velocity data for one of the periodic SSAM increases beginning 20 August and the step change on 18 September (Figure 8B–8C). In both cases, the dominant signal in the 0.5–1.5 Hz range is centered just below 1 Hz. This signal decreases in frequency and increases in power at the onset of the periodic SSAM fluctuation; it increases in frequency and decreases in power after the earth-

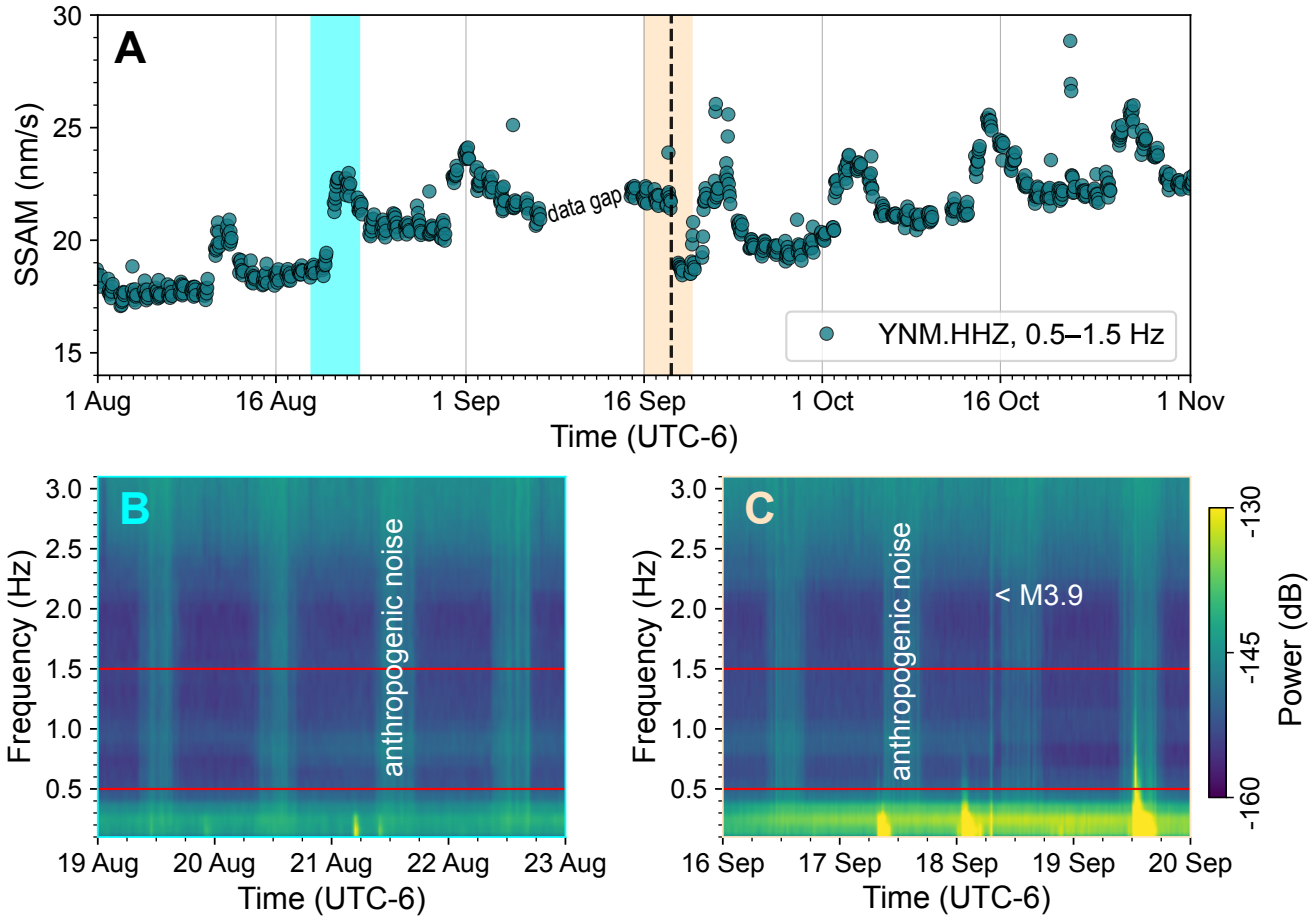

Figure 8: SSAM and spectrograms related to vertical velocity data at station YNM. [A] Overnight SSAM for 1-hour segments in the 0.5–1.5 Hz band during August–October 2022. There is a step change after the M3.9 earthquake (black dashed line). [B] Spectrogram for 19–23 August corresponding to the blue box in [A]. The periodic SSAM signal is related to a small decrease in peak frequency and slight increase in power between 0.5–2.0 Hz. [C] Spectrogram for 16–20 September corresponding to the light orange box in [A]. After the earthquake, there is a small increase in peak frequency and a subtle decrease in power between 0.7–2.2 Hz. The three low-frequency signals are due to teleseismic earthquakes. Spectrograms in [B] and [C] show power clipped to -160 and -130 dB and red lines encapsulate the 0.5–1.5 Hz band.

quake. We note that significant decreases in SSAM at this frequency range are not unique to the M3.9 event and have occurred multiple times prior to and during Steamboat's active phase; however, they were not associated with frequency shifts [Reed et al. 2021]. Because the 0.5–1.5 Hz tremor weakened almost immediately following the earthquake and was accompanied by downward frequency shifts in other signals (>27 Hz in Figure 4C), we argue the changes in 0.5–1.5 Hz tremor can reasonably be attributed to processes triggered by the earthquake.

4.3 Subsurface relative seismic velocity

Were there changes to subsurface properties? Local earthquakes are thought to decrease seismic velocity in hydrothermal areas by clearing fractures during pore pressure fluctuations [e.g. Brodsky et al. 2003; Manga et al. 2012]. We can apply ambient noise seismic interferometry [e.g. Brenguier et al. 2008; Snieder and Larose 2013] using the three-component YNM data to obtain relative seismic velocity changes (dv/v) of subsurface media. We focus our analysis on the month of September 2022 and compute noise cross-correlation functions (NCFs) in four different frequency bands (0.5–1.5, 1.5–2.5, 2.5–3.5, and 3.5–4.5 Hz) using MSNoise [Lecocq et al. 2014].

Our data processing methods are similar to those described in Brenguier et al. [2008] and Taira et al. [2018]. First, we correct instrument response on 24-hour continuous data slices to obtain ground displacement and apply a bandpass filter between 0.08 and 8.0 Hz. Daily bandpass-filtered recordings are then down-sampled from 100 to 20 Hz and split into 30-minute sections. Following Hobiger et al. [2014], we compute NCFs for cross-component pairs (i.e. vertical-north, vertical-east, and north-east) where a spectral whitening process can be applied to minimize signals associated with local and teleseismic earthquakes. Subsequently, one-bit normalization is applied at the frequency bands of interest.

We measure temporal change in dv/v through the time delay estimate (dt) for a pair of NCFs with the moving window

cross-spectral technique [Clarke et al. 2011], assuming a homogeneous velocity where

$$\frac{dv}{v} = -\frac{dt}{t}. \quad (5)$$

We only use dt in a moving window where the value of cross-correlation between the stacked and reference NCFs exceeds 0.85. The windows overlap by 50 % and the window lengths are equivalent to the longest period in each frequency band used. Our analysis focuses on a 3 s coda of NCFs (–5 to –2 s and 2 to 5 s) to measure time delays between the 60, 120, 240, and 360-minute stacks of NCFs and reference NCFs computed for data between December 2021 and December 2022.

A sudden dv/v reduction of $\sim 3 \pm 1$ % following the M3.9 earthquake appears in the 1.5–2.5 Hz frequency band when using 60- and 120-minute stacking (Figure 9). The decrease in dv/v for the 1.5–2.5 Hz band is not present in the 240- and 360-minute stacking results, which supports prompt recovery of seismic velocity. Though the uncertainties are large and there are other sudden, unexplained variations in dv/v up to 1.5 % for this band in September, the timing and magnitude of the ~3 % velocity reduction stand out. Our analysis did not find sudden dv/v changes after the earthquake in the 0.5–1.5, 2.5–3.5, and 3.5–4.5 Hz bands for any of our stacking methods. This suggests the change in seismic velocity occurred at a narrow depth interval. Assuming that the codas of our NCFs are dominated by Rayleigh waves and the ratio of P-wave to S-wave velocity (v_p/v_s) is 1.6 [Husen et al. 2004], we calculate a surface wave sensitivity kernel with a 1D P-wave velocity model used by the University of Utah Seismograph Stations to determine earthquake locations (Figure 10). We find that the reduction in relative seismic velocity likely occurred at a depth of 300–500 m given the lack of dv/v changes in frequency bands other than 1.5–2.5 Hz.

5 Discussion

Overall, we find it plausible that Steamboat's major eruption on 18 September 2022 was earthquake-triggered. The low probability of eruption on that day is encouraging but does not prove the eruption was related to the earthquake. We established that the M3.9 earthquake produced a PGV of 1.2 cm s^{-1} and that no other analyzed earthquake produced ground motions >1 cm s^{-1} since the active phase began. The immediate post-earthquake reductions in SSAM and dv/v indicate changes in subsurface properties and shed light on a triggering mechanism.

Previous studies that documented temporary decreases of dv/v following local and teleseismic earthquakes at volcanoes [e.g. Brenguier et al. 2014; Lesage et al. 2014; Nimiya et al. 2017] and hydrothermal systems [e.g. Taira and Brenguier 2016; Taira et al. 2018; Saade et al. 2019] have attributed the drop in seismic velocity to the opening of cracks. The relationship between peak dynamic stress, PDS, and peak ground velocity is

$$\mathrm{PDS} = G\frac{\mathrm{PGV}}{v_s}, \quad (6)$$

where G is the shear modulus [Hill et al. 1993; van der Elst and Brodsky 2010]. Using representative values of G = 13 GPa and v_s = 2.3 km s^{-1} for water-saturated silica sinter [Muñoz-Saez et al. 2016], the M3.9 earthquake generated a peak dynamic stress of ~0.07 MPa. While larger than those from solid Earth tides and barometric pressure changes, this stress is likely too low to promote new fracture formation because it does not exceed the tensile or compressive strength of rock (see Appendix E in Gudmundsson [2020]). The quick recovery of dv/v (hours vs. weeks to months) further implies that there were no permanent changes in rock properties. Instead, the decrease in velocity perhaps resulted from an increase in gas fraction or decrease in water levels which would raise the bulk rock compressibility.

There are physical and thermal mechanisms that enable earthquakes to trigger eruptions without the need for new fractures. Simply disturbing the pool of some thermal features can trigger boiling or eruptions; historically, tourists sometimes induced eruptions by throwing soap [e.g. Hague 1889; Graham 1893; Pálmason 2002] or objects [e.g. Allen and Day 1935] into geysers. Vibrations have also been shown to trigger bubble nucleation and eruption in laboratory geysers [Steinberg et al. 1982]. In these examples, the water must be superheated or primed to erupt so that nucleating bubbles or promoting convection is sufficient to initiate an eruption [Rinehart 1974]. However, the 8.25-hour delay between earthquake and eruption at Steamboat is too long to favor these mechanisms. There are other examples where changes to geysers occur gradually. After the 2002 M7.9 Denali earthquake, Daisy Geyser's eruption intervals decreased from a variable 2.3–3.5 hours to a consistent 1.5–1.7 hours over a 24-hour period [Husen et al. 2004; Hurwitz et al. 2014]. The recovery to its pre-earthquake state occurred more gradually over several months. This is in line with some other hydrogeological responses in groundwater levels [e.g. Brodsky et al. 2003; Roeloffs et al. 2003; Shi et al. 2015] and streamflow [e.g. Muir-Wood and King 1993; Manga 2001; Wang and Manga 2015] that take days to weeks to reach their peak and then recover to pre-earthquake conditions over months.

Our proposed eruption triggering at Steamboat would be best explained by earthquake-induced changes in hydraulic head or subsurface permeability [Ingebritsen and Rojstaczer 1996] that affect fluid and heat flow. Existing fractures just north of Steamboat, identified from geologic mapping and airborne infrared surveys, trend roughly toward YNM [White et al. 1988; Jaworowski et al. 2006]. If the earthquake affected subsurface permeability, the decrease in relative seismic velocity could represent fluid and thus heat flow away from a 300–500 m deep reservoir, perhaps toward Steamboat along these fractures. The persistent, ~1 Hz tremor band identified from SSAM could be interpreted as resonance of or boiling within a separate fluid-filled conduit or cavity. If boiling decreased and/or the fluid level dropped, this might explain the observed increase in resonant frequency [Rudolph et al. 2018; Teshima et al. 2022]. The increased distance between YNM and the fluid-filled part of the conduit and/or the reduction in boiling would then explain the weakening tremor.

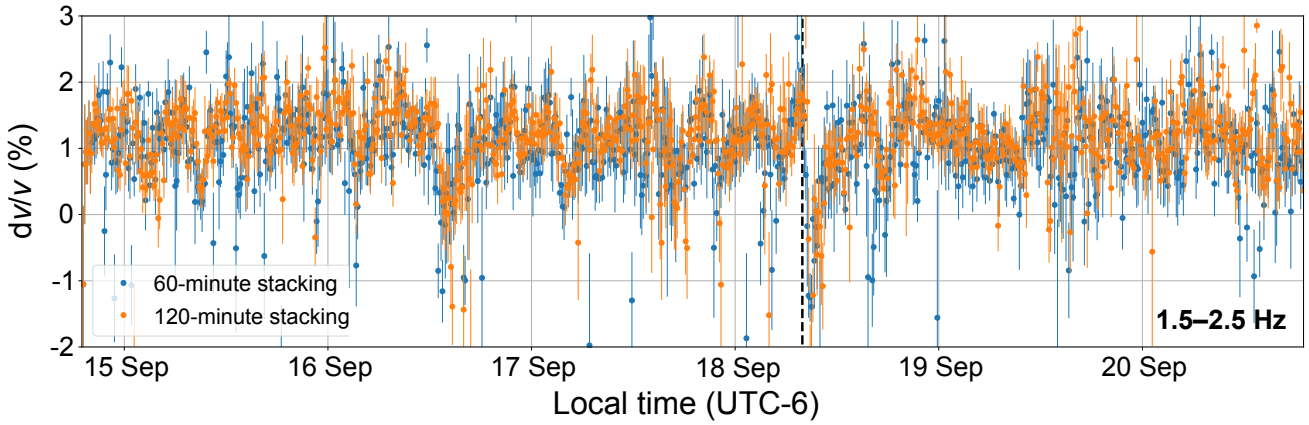

Figure 9: Relative velocity changes (dv/v) with error bars extending to ± 2 standard deviations for a frequency band of 1.5–2.5 Hz in the days around the M3.9 earthquake (black dashed line). Both 60-minute (blue) and 120-minute (orange) stacking methods show a decrease in dv/v immediately following the earthquake, though there are other unexplained variations like that on 16 September at midday. The second largest PGV (0.8 cm s^{-1}) during the active phase occurred on 19 September just before 12:23 without a corresponding decrease in dv/v.

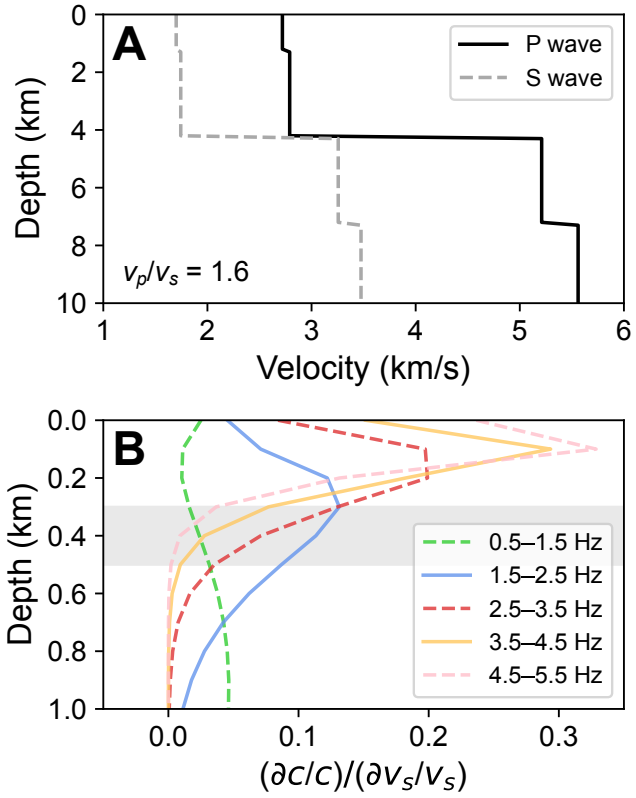

Figure 10: [A] Velocity model assuming v_p/v_s is 1.6 [Husen et al. 2004]. [B] Sensitivity kernel calculated from the velocity model in [A], assuming the coda of NCFs is dominated by Rayleigh waves. Because the decrease in *dv/v* appears only in the 1.5–2.5 Hz results, we infer the change most likely occurred at 300–500 m depth (grey shaded area) where the sensitivity to 1.5–2.5 Hz is highest relative to the other frequencies.

The reasons for why geysers react to some earthquakes but not others remain elusive. We restricted our PGV analysis to earthquakes during Steamboat's active phase, but Norris Geyser Basin has experienced greater dynamic stresses from local and regional earthquakes prior to March 2018. Most recently, a local M_w 4.8 earthquake produced a PGV of >3 cm s^{-1} at YNM in 2014 but did not trigger an eruption [Reed et al. 2021]. There was a step change reduction in 0.5–1.5 Hz SSAM after this event but, unlike after the 2022 M3.9 earthquake, the peak frequency remained constant (Supplementary Material 2 Figure S3)]. No major eruptions were recorded following any of five ≥M5 earthquakes that occurred within 15 km of Norris in 1975 and 1976. For completeness, we note there exists an unconfirmed logbook report of steam phase behavior at Steamboat two days after the 30 June 1975 Yellowstone National Park earthquake [Bellingham 2023], but we choose to discount it because it is not referenced in the more authoritative records from that year. The more distant 1983 M_w 6.9 Borah Peak earthquake affected geyser activity in a localized area of the Upper Geyser Basin [Hutchinson 1985], but we found no records of effects at Norris and again, there was no reported Steamboat eruption. Even the 1959 M_w 7.3 Hebgen Lake earthquake, which triggered eruptions in dormant geysers and springs with no known eruptive history across Yellowstone and increased turbidity in Norris thermal features [White et al. 1988], failed to elicit an eruption of Steamboat.

Studies of volcanic eruptions indicate that the internal state of a volcano is a primary control on whether or not an earthquake-triggered eruption occurs [e.g. Bebbington and Marzocchi 2011; Sawi and Manga 2018; Farías and Basualto 2020]. This is likely true of geysers as well. None of the earthquakes mentioned above except for the Borah Peak earthquake coincided with Steamboat active phases, and we speculate that earthquake-triggering might only be possible at Steamboat when the local system is capable of frequent major eruptions. Steamboat erupted just 6 more times in 13 months following the Borah Peak earthquake before reentering dormancy; a lack of response to that event might imply that the

Steamboat system was already headed toward dormancy at the time.

6 Conclusion

On 18 September 2022, Steamboat Geyser erupted just 8.25 hours after a nearby M3.9 earthquake. We conclude it is more likely than not that this eruption was triggered by the earthquake for the following reasons:

1. There is a low probability that the eruption occurred on the day of the earthquake by chance based on Fréchet modeling of the eruption interval population.

2. The 1.2 cm s^{-1} PGV recorded at YNM is the greatest experienced at Norris Geyser Basin during Steamboat's recent active phase. It also exceeds a 1 cm s^{-1} threshold associated with earthquake-related responses at other geysers, mud volcanoes, and streams.

3. Seismic data suggest possible subsurface hydrothermal changes following the earthquake, supporting the feasibility of a response from Steamboat. While the surface discharge of monitored Norris thermal features did not change, our SSAM results suggest a weakening or deepening of a 0.5–1.5 Hz tremor source and our dv/v results indicate a short-lived velocity reduction in material at 300–500 m depth.

However, we keep in mind these corresponding caveats:

1. Low chance of coincidence does not mean a coincidence is impossible. The 90-day interval before this eruption is an outlier in the ongoing active phase which makes an interval distribution-based probability analysis somewhat less compelling.

2. There are no historical reports of Steamboat Geyser having major eruptions following other energetic local or regional earthquakes. It is possible that earthquake-triggering can only occur at Steamboat during active phases; however, the 1983 M6.9 Borah Peak earthquake failed to trigger an eruption during Steamboat's 1980s active phase despite affecting other Yellowstone geysers.

3. More work is needed to understand the source mechanism of the 0.5–1.5 Hz tremor and how changes in frequency and amplitude may relate to an eruption triggering mechanism. Additionally, probing relative seismic velocity changes at such short timescales is difficult as less noise can be removed via stacking. The dv/v reduction we found was not much larger than background variations.

Finally, this analysis was only possible due to the number of monitoring instruments at Norris Geyser Basin. The installation of more seismometers and eruption recording equipment in hydrothermal areas would increase the chance of identifying earthquake-triggered eruptions when they occur and allow documentation of the accompanying subsurface changes.

Author Contributions

MHR: Conceptualization, Formal analysis (PGV, eruption interval, eruption volume, and SSAM calculations), Writing - Original Draft, Writing - Review & Editing, Visualization; AB: Conceptualization, Formal analysis (Fréchet modeling), Writing - Original Draft, Writing - Review & Editing, Visualization; TT: Formal analysis (dv/v and sensitivity kernel), Writing - Original Draft, Writing - Review & Editing, Visualization; JF: Resources (1D velocity model), Writing - Review & Editing; MM: Conceptualization, Writing - Original Draft, Writing - Review & Editing.

Acknowledgements

We thank Graham Meech for the wonderful photo of Steamboat and MA Bellingham for her assistance in assessing the quality of Whirligig data. Two anonymous reviewers provided comments that greatly improved the organization of this manuscript. We also thank the University of Utah and the U.S. Geological Survey for maintaining instruments in Yellowstone. Financial support for this work came from NSF Grant EAR2116573, the Northern California Chapter of the ARCS Foundation, the Miller Institute for Basic Research in Science, and CIFAR Earth 4D.

Data Availability

GeyserTimes data are available via https://geysertimes.org/retrieve.php. The Yellowstone Seismic Network (network code WY) is operated by the University of Utah Seismograph Stations and seismic data are made available through the EarthScope Consortium Data Management Center (https://ds.iris.edu/ds/nodes/dmc/). Earthquake data come from the ANSS Comprehensive Catalog published by the U.S. Geological Survey (https://earthquake.usgs.gov/data/comcat/). The Tantalus Creek streamgage is operated jointly by the U.S. Geological Survey and the U.S. National Park Service; discharge data is available at https://waterdata.usgs.gov/monitoring-location/06036940. Telemetered temperature sensors are maintained by the Yellowstone Volcano Observatory and the raw data used in this study are attached in Supplementary Material 1.

References

Allen, E. T. and A. L. Day (1935). *Hot springs of the Yellowstone National Park*. https://catalog.hathitrust.org/Record/001639423. Carnegie Institution of Washington.

Barth, T. F. W. (1950). *Volcanic geology, hot springs, and geysers of Iceland*. https://catalog.hathitrust.org/Record/001639486. Carnegie Institution of Washington.

Bebbington, M. S. and W. Marzocchi (2011). "Stochastic models for earthquake triggering of volcanic eruptions". *Jour-*

nal of Geophysical Research 116(B5). DOI: 10.1029/2010jb008114.

Bellingham, M. (2023). *Note ID 32609 [database entry; transcription of entry in the 1975 Norris Geyser Basin logbook]*. https://geysertimes.org/note.php?id=32609. GeyserTimes.

Beverly, C. (2022). *Eruption ID 1384597 [database entry]*. https://geysertimes.org/eruption.php?id=1384597. GeyserTimes.

– (2023). *Note ID 27844 [database entry]*. https://geysertimes.org/note.php?id=27844. GeyserTimes.

Bonini, M., M. L. Rudolph, and M. Manga (2016). "Long- and short-term triggering and modulation of mud volcano eruptions by earthquakes". *Tectonophysics* 672–673, pages 190–211. DOI: 10.1016/j.tecto.2016.01.037.

Brenguier, F., M. Campillo, T. Takeda, Y. Aoki, N. M. Shapiro, X. Briand, K. Emoto, and H. Miyake (2014). "Mapping pressurized volcanic fluids from induced crustal seismic velocity drops". *Science* 345(6192), pages 80–82. DOI: 10.1126/science.1254073.

Brenguier, F., N. M. Shapiro, M. Campillo, V. Ferrazzini, Z. Duputel, O. Coutant, and A. Nercessian (2008). "Towards forecasting volcanic eruptions using seismic noise". *Nature Geoscience* 1(2), pages 126–130. DOI: 10.1038/ngeo104.

Brodsky, E. E. and S. G. Prejean (2005). "New constraints on mechanisms of remotely triggered seismicity at Long Valley Caldera". *Journal of Geophysical Research: Solid Earth* 110(B4). DOI: 10.1029/2004jb003211.

Brodsky, E. E., E. Roeloffs, D. Woodcock, I. Gall, and M. Manga (2003). "A mechanism for sustained groundwater pressure changes induced by distant earthquakes". *Journal of Geophysical Research: Solid Earth* 108(B8). DOI: 10.1029/2002jb002321.

Clarke, D., L. Zaccarelli, N. M. Shapiro, and F. Brenguier (2011). "Assessment of resolution and accuracy of the Moving Window Cross Spectral technique for monitoring crustal temporal variations using ambient seismic noise: MWCS: assessment of resolution and accuracy". *Geophysical Journal International* 186(2), pages 867–882. DOI: 10.1111/j.1365-246x.2011.05074.x.

Cros, E., P. Roux, J. Vandemeulebrouck, and S. Kedar (2011). "Locating hydrothermal acoustic sources at Old Faithful Geyser using Matched Field Processing: Old Faithful viewed through array processing". *Geophysical Journal International* 187(1), pages 385–393. DOI: 10.1111/j.1365-246x.2011.05147.x.

Dawson, P. B., M. C. Benítez, J. B. Lowenstern, and B. A. Chouet (2012). "Identifying bubble collapse in a hydrothermal system using hidden Markov models". *Geophysical Research Letters* 39(1). DOI: 10.1029/2011gl049901.

De la Cruz-Reyna, S., M. Tárraga, R. Ortiz, and A. Martínez-Bringas (2010). "Tectonic earthquakes triggering volcanic seismicity and eruptions. Case studies at Tungurahua and Popocatépetl volcanoes". *Journal of Volcanology and Geothermal Research* 193(1–2), pages 37–48. DOI: 10.1016/j.jvolgeores.2010.03.005.

Eibl, E. P. S., D. Müller, T. R. Walter, M. Allahbakhshi, P. Jousset, G. P. Hersir, and T. Dahm (2021). "Eruptive Cycle and Bubble Trap of Strokkur Geyser, Iceland". *Journal of Geophysical Research: Solid Earth* 126(4). DOI: 10.1029/2020jb020769.

Farías, C. and D. Basualto (2020). "Reactivating and Calming Volcanoes: The 2015 MW 8.3 Illapel Megathrust Strike". *Geophysical Research Letters* 47(16). DOI: 10.1029/2020gl087738.

Farrell, J., S. Husen, and R. B. Smith (2009). "Earthquake swarm and b-value characterization of the Yellowstone volcano-tectonic system". *Journal of Volcanology and Geothermal Research* 188(1–3), pages 260–276. DOI: 10.1016/j.jvolgeores.2009.08.008.

Farrell, J., R. B. Smith, T. Taira, W.-L. Chang, and C. M. Puskas (2010). "Dynamics and rapid migration of the energetic 2008–2009 Yellowstone Lake earthquake swarm". *Geophysical Research Letters* 37(19). DOI: 10.1029/2010gl044605.

Friedman, I. (2007). "Monitoring changes in geothermal activity at Norris Geyser Basin by satellite telemetry, Yellowstone National Park, Wyoming". *Integrated geoscience studies in the Greater Yellowstone Area—Volcanic, tectonic, and hydrothermal processes in the Yellowstone geoecosystem*. Edited by L. A. Morgan. U.S. Geological Survey Professional Paper 1717. U. S. Geological Survey, pages 509–532. DOI: 10.3133/pp1717.

Graham, J. C. (1893). "Some experiments with an artificial geyser". *American Journal of Science* s3-45(265), pages 54–60. DOI: 10.2475/ajs.s3-45.265.54.

Gudmundsson, A. (2020). "Understanding the structure, deformation and dynamics of volcanoes". *Volcanotectonics*. Edited by A. Gudmundsson. Cambridge University Press, pages 568–571. DOI: 10.1017/9781139176217.016.

Hague, A. (1889). "Soaping Geysers". *Science* ns-13(328), pages 382–384. DOI: 10.1126/science.ns-13.328.382.b.

Havskov, J. and G. Alguacil (2016). "Correction for Instrument Response". *Instrumentation in Earthquake Seismology*. Springer International Publishing, pages 197–230. ISBN: 9783319213149. DOI: 10.1007/978-3-319-21314-9_6.

Hill, D. P., P. A. Reasenberg, A. Michael, W. J. Arabaz, G. Beroza, D. Brumbaugh, J. N. Brune, R. Castro, S. Davis, D. dePolo, W. L. Ellsworth, J. Gomberg, S. Harmsen, L. House, S. M. Jackson, M. J. S. Johnston, L. Jones, R. Keller, S. Malone, L. Munguia, S. Nava, J. C. Pechmann, A. Sanford, R. W. Simpson, R. B. Smith, M. Stark, M. Stickney, A. Vidal, S. Walter, V. Wong, and J. Zollweg (1993). "Seismicity Remotely Triggered by the Magnitude 7.3 Landers, California, Earthquake". *Science* 260(5114), pages 1617–1623. DOI: 10.1126/science.260.5114.1617.

Hobiger, M., U. Wegler, K. Shiomi, and H. Nakahara (2014). "Single-station cross-correlation analysis of ambient seismic noise: application to stations in the surroundings of the 2008 Iwate-Miyagi Nairiku earthquake". *Geophysical Journal International* 198(1), pages 90–109. DOI: 10.1093/gji/ggu115.

Hurwitz, S., M. Manga, K. Campbell, C. Muñoz-Saez, and E. Eibl (2021). "Why Study Geysers?" *Eos* 102. DOI: 10.1029/2021eo161365.

Hurwitz, S., R. A. Sohn, K. Luttrell, and M. Manga (2014). "Triggering and modulation of geyser eruptions in Yellowstone National Park by earthquakes, earth tides, and weather". *Journal of Geophysical Research: Solid Earth* 119(3), pages 1718–1737. DOI: 10.1002/2013jb010803.

Husen, S., R. Taylor, R. Smith, and H. Healser (2004). "Changes in geyser eruption behavior and remotely triggered seismicity in Yellowstone National Park produced by the 2002 M 7.9 Denali fault earthquake, Alaska". *Geology* 32(6), page 537. DOI: 10.1130/g20381.1.

Hutchinson, R. A. (1985). "Hydrothermal changes in the Upper Geyser Basin, Yellowstone National Park, after the 1983 Borah Peak, Idaho, earthquake". *Proceedings of workshop XXVIII on the Borah Peak, Idaho earthquake*. Open-File Report 85-290-A, pages 612–624. DOI: 10.3133/ofr85290a.

Ingebritsen, S. E. and S. A. Rojstaczer (1996). "Geyser periodicity and the response of geysers to deformation". *Journal of Geophysical Research: Solid Earth* 101(B10), pages 21891–21905. DOI: 10.1029/96jb02285.

Iyer, H. M. and T. Hitchcock (1974). "Seismic noise measurements in Yellowstone National Park". *Geophysics* 39(4), pages 389–400. DOI: 10.1190/1.1440437.

Jaworowski, C., H. P. Heasler, C. C. Hardy, and L. P. Queen (2006). *Control of hydrothermal fluids by natural fractures at Norris Geyser Basin*. https://www.volcano.gov/vsc/file_mngr/file-25/JaworowskiYellSciFall06.pdf. Yellowstone Science.

Kedar, S., H. Kanamori, and B. Sturtevant (1998). "Bubble collapse as the source of tremor at Old Faithful Geyser". *Journal of Geophysical Research: Solid Earth* 103(B10), pages 24283–24299. DOI: 10.1029/98jb01824.

Kieffer, S. W. (1984). "Seismicity at Old Faithful Geyser: an isolated source of geothermal noise and possible analogue of volcanic seismicity". *Journal of Volcanology and Geothermal Research* 22(1–2), pages 59–95. DOI: 10.1016/0377-0273(84)90035-0.

Lecocq, T., C. Caudron, and F. Brenguier (2014). "MSNoise, a Python Package for Monitoring Seismic Velocity Changes Using Ambient Seismic Noise". *Seismological Research Letters* 85(3), pages 715–726. DOI: 10.1785/0220130073.

Legaz, A., A. Revil, P. Roux, J. Vandemeulebrouck, P. Gouédard, T. Hurst, and A. Bolève (2009). "Self-potential and passive seismic monitoring of hydrothermal activity: A case study at Iodine Pool, Waimangu geothermal valley, New Zealand". *Journal of Volcanology and Geothermal Research* 179(1–2), pages 11–18. DOI: 10.1016/j.jvolgeores.2008.09.015.

Lesage, P., G. Reyes-Dávila, and R. Arámbula-Mendoza (2014). "Large tectonic earthquakes induce sharp temporary decreases in seismic velocity in Volcán de Colima, Mexico". *Journal of Geophysical Research: Solid Earth* 119(5), pages 4360–4376. DOI: 10.1002/2013jb010884.

Linde, A. T. and I. S. Sacks (1998). "Triggering of volcanic eruptions". *Nature* 395(6705), pages 888–890. DOI: 10.1038/27650.

Liu, C.-N., F.-C. Lin, M. Manga, J. Farrell, S.-M. Wu, M. H. Reed, A. Barth, J. Hungerford, and E. White (2023). "Thumping Cycle Variations of Doublet Pool in Yellowstone National Park, USA". *Geophysical Research Letters* 50(4). DOI: 10.1029/2022gl101175.

Manga, M. (2001). "Origin of postseismic streamflow changes inferred from baseflow recession and magnitude-distance relations". *Geophysical Research Letters* 28(10), pages 2133–2136. DOI: 10.1029/2000gl012481.

Manga, M., I. Beresnev, E. E. Brodsky, J. E. Elkhoury, D. Elsworth, S. E. Ingebritsen, D. C. Mays, and C.-Y. Wang (2012). "Changes in permeability caused by transient stresses: Field observations, experiments, and mechanisms". *Reviews of Geophysics* 50(2). DOI: 10.1029/2011rg000382.

Marler, G. D. and D. E. White (1975). "Seismic Geyser and Its Bearing on the Origin and Evolution of Geysers and Hot Springs of Yellowstone National Park". *Geological Society of America Bulletin* 86(6), page 749. DOI: 10.1130/0016-7606(1975)86<749:sgaibo>2.0.co;2.

Mellors, R., D. Kilb, A. Aliyev, A. Gasa11, and G. Yetirmishli (2007). "Correlations between earthquakes and large mud volcano eruptions". *Journal of Geophysical Research: Solid Earth* 112(B4). DOI: 10.1029/2006jb004489.

Mogi, K. (1963). "Some discussions on aftershocks, foreshocks and earthquake swarms-the fracture of a semi finite body caused by an inner stress origin and its relation to the earthquake phenomena". *Bulletin of the Earthquake Research Institute* 41, pages 615–658.

Muir-Wood, R. and G. C. P. King (1993). "Hydrological signatures of earthquake strain". *Journal of Geophysical Research: Solid Earth* 98(B12), pages 22035–22068. DOI: 10.1029/93jb02219.

Muñoz-Saez, C., S. Saltiel, M. Manga, C. Nguyen, and H. Gonnermann (2016). "Physical and hydraulic properties of modern sinter deposits: El Tatio, Atacama". *Journal of Volcanology and Geothermal Research* 325, pages 156–168. DOI: 10.1016/j.jvolgeores.2016.06.026.

Nayak, A., M. Manga, S. Hurwitz, A. Namiki, and P. B. Dawson (2020). "Origin and Properties of Hydrothermal Tremor at Lone Star Geyser, Yellowstone National Park, USA". *Journal of Geophysical Research: Solid Earth* 125(12). DOI: 10.1029/2020jb019711.

Nimiya, H., T. Ikeda, and T. Tsuji (2017). "Spatial and temporal seismic velocity changes on Kyushu Island during the 2016 Kumamoto earthquake". *Science Advances* 3(11). DOI: 10.1126/sciadv.1700813.

Nishimura, T. (2017). "Triggering of volcanic eruptions by large earthquakes". *Geophysical Research Letters* 44(15), pages 7750–7756. DOI: 10.1002/2017gl074579.

Pálmason, G. (2002). "Iceland's Geysir aroused by earthquakes in June 2000". *The GOSA Transactions* 7, pages 139–147.

Reed, M. H. and M. Manga (2023). "Snow Suppresses Seismic Signals From Steamboat Geyser". *Geophysical Research Letters* 50(12). DOI: 10.1029/2023gl103904.

Reed, M. H., C. Muñoz-Saez, S. Hajimirza, S.-M. Wu, A. Barth, T. Girona, M. Rasht-Behesht, E. B. White, M. S. Karplus, S. Hurwitz, and M. Manga (2021). "The 2018 reawakening and eruption dynamics of Steamboat Geyser, the world's tallest active geyser". *Proceedings of the National Academy of Sciences* 118(2). DOI: 10.1073/pnas.2020943118.

Rinehart, J. S. (1974). "Geysers". *Eos, Transactions American Geophysical Union* 55(12), pages 1052–1062. DOI: 10.1029/eo055i012p01052.

Roeloffs, E., M. Sneed, D. L. Galloway, M. L. Sorey, C. D. Farrar, J. F. Howle, and J. Hughes (2003). "Water-level changes induced by local and distant earthquakes at Long Valley caldera, California". *Journal of Volcanology and Geothermal Research* 127(3–4), pages 269–303. DOI: 10.1016/s0377-0273(03)00173-2.

Rogers, J. and C. Stephens (1995). "SSAM: real-time seismic spectral amplitude measurement on a PC and its application to volcano monitoring". *Bulletin of the Seismological Society of America* 85(2), pages 632–639. DOI: 10.1785/BSSA0850020632.

Rudolph, M. L. and M. Manga (2012). "Frequency dependence of mud volcano response to earthquakes". *Geophysical Research Letters* 39(14). DOI: 10.1029/2012gl052383.

Rudolph, M. L., R. A. Sohn, and E. Lev (2018). "Fluid oscillations in a laboratory geyser with a bubble trap". *Journal of Volcanology and Geothermal Research* 368, pages 100–110. DOI: 10.1016/j.jvolgeores.2018.11.003.

Saade, M., K. Araragi, J. P. Montagner, E. Kaminski, P. Roux, Y. Aoki, and F. Brenguier (2019). "Evidence of reactivation of a hydrothermal system from seismic anisotropy changes". *Nature Communications* 10(1). DOI: 10.1038/s41467-019-13156-8.

Sawi, T. M. and M. Manga (2018). "Revisiting short-term earthquake triggered volcanism". *Bulletin of Volcanology* 80(7). DOI: 10.1007/s00445-018-1232-2.

Seropian, G., B. M. Kennedy, T. R. Walter, M. Ichihara, and A. D. Jolly (2021). "A review framework of how earthquakes trigger volcanic eruptions". *Nature Communications* 12(1). DOI: 10.1038/s41467-021-21166-8.

Shelly, D. R., D. P. Hill, F. Massin, J. Farrell, R. B. Smith, and T. Taira (2013). "A fluid-driven earthquake swarm on the margin of the Yellowstone caldera". *Journal of Geophysical Research: Solid Earth* 118(9), pages 4872–4886. DOI: 10.1002/jgrb.50362.

Shi, Z., G. Wang, M. Manga, and C.-Y. Wang (2015). "Mechanism of co-seismic water level change following four great earthquakes – insights from co-seismic responses throughout the Chinese mainland". *Earth and Planetary Science Letters* 430, pages 66–74. DOI: 10.1016/j.epsl.2015.08.012.

Snieder, R. and E. Larose (2013). "Extracting Earth's Elastic Wave Response from Noise Measurements". *Annual Review of Earth and Planetary Sciences* 41(1), pages 183–206. DOI: 10.1146/annurev-earth-050212-123936.

Steinberg, G. S., A. G. Merzhanov, and A. S. Steinberg (1982). "Geyser process; its theory, modeling, and field experiment. Part 4. On seismic influence on geyser regime". *Modern Geology* 8, pages 79–86.

Taira, T. and F. Brenguier (2016). "Response of hydrothermal system to stress transients at Lassen Volcanic Center, California, inferred from seismic interferometry with ambient noise". *Earth, Planets and Space* 68(1). DOI: 10.1186/s40623-016-0538-6.

Taira, T., A. Nayak, F. Brenguier, and M. Manga (2018). "Monitoring reservoir response to earthquakes and fluid extraction, Salton Sea geothermal field, California". *Science Advances* 4(1). DOI: 10.1126/sciadv.1701536.

Teshima, N., A. Tora3u, and M. Ichihara (2022). "Precursory pressure oscillation in a laboratory geyser system". *Journal of Volcanology and Geothermal Research* 429, page 107613. DOI: 10.1016/j.jvolgeores.2022.107613.

Thorkelsson, T. (1940). *On thermal activity in Iceland and geyser action*. Volume 25. Ísafoldarprentsmiđja.

University of Utah Seismograph Stations (2022). *M 3.9—22 km SSW of Mammoth, Wyoming [dataset]*. https://earthquake.usgs.gov/earthquakes/eventpage/uu60515582/origin/detail. Advanced National Seismic System Comprehensive Catalog.

Van der Elst, N. J. and E. E. Brodsky (2010). "Connecting near-field and far-field earthquake triggering to dynamic strain". *Journal of Geophysical Research: Solid Earth* 115(B7). DOI: 10.1029/2009jb006681.

Vandemeulebrouck, J., R. A. Sohn, M. L. Rudolph, S. Hurwitz, M. Manga, M. J. S. Johnston, S. A. Soule, D. McPhee, J. M. G. Glen, L. Karlstrom, and F. Murphy (2014). "Eruptions at Lone Star geyser, Yellowstone National Park, USA: 2. Constraints on subsurface dynamics". *Journal of Geophysical Research: Solid Earth* 119(12), pages 8688–8707. DOI: 10.1002/2014jb011526.

Vander Ley, B. (2021). "Measuring the height of Steamboat Geyser in 2020, plus additional data". *The Geyser Gazer Sput* 35(2), pages 17–22.

Waite, G. P. and R. B. Smith (2002). "Seismic evidence for fluid migration accompanying subsidence of the Yellowstone caldera". *Journal of Geophysical Research: Solid Earth* 107(B9). DOI: 10.1029/2001jb000586.

Walter, T. R., R. Wang, M. Zimmer, H. Grosser, B. Lühr, and A. Ratdomopurbo (2007). "Volcanic activity influenced by tectonic earthquakes: Static and dynamic stress triggering at Mt. Merapi". *Geophysical Research Letters* 34(5). DOI: 10.1029/2006gl028710.

Walter, T. R. and F. Amelung (2007). "Volcanic eruptions following M ≥ 9 megathrust earthquakes: Implications for the Sumatra-Andaman volcanoes". *Geology* 35(6), page 539. DOI: 10.1130/g23429a.1.

Wang, C.-Y. and M. Manga (2015). "New streams and springs after the 2014 Mw6.0 South Napa earthquake". *Nature Communications* 6(1). DOI: 10.1038/ncomms8597.

– (2021). *Water and Earthquakes*. Springer International Publishing. ISBN: 9783030643089. DOI: 10.1007/978-3-030-64308-9.

White, E. D., R. A. Hutchison, and T. E. C. Keith (1988). *The geology and remarkable thermal activity of Norris Geyser Basin, Yellowstone National Park, Wyoming*. U. S. Geological Survey Professional Paper 1456. U. S. Geological Survey.

Wolf, M. (2022). *Note ID 23890 [database entry]*. https://geysertimes.org/note.php?id=23890. GeyserTimes.

Wu, S.-M., F.-C. Lin, J. Farrell, and A. Allam (2019). "Imaging the Deep Subsurface Plumbing of Old Faithful Geyser From Low-Frequency Hydrothermal Tremor Migration". *Geophysical Research Letters* 46(13), pages 7315–7322. DOI: 10.1029/2018gl081771.

Wu, S.-M., F.-C. Lin, J. Farrell, W. E. Keller, E. B. White, and J. D. G. Hungerford (2021). "Imaging the Subsurface Plumbing Complex of Steamboat Geyser and Cistern Spring With Hydrothermal Tremor Migration Using Seismic Interferometry". *Journal of Geophysical Research: Solid Earth* 126(4). DOI: 10.1029/2020jb021128.

Wu, S.-M., K. M. Ward, J. Farrell, F.-C. Lin, M. Karplus, and R. B. Smith (2017). "Anatomy of Old Faithful From Subsurface Seismic Imaging of the Yellowstone Upper Geyser Basin". *Geophysical Research Letters* 44(20). DOI: 10.1002/2017gl075255.

Yellowstone Volcano Observatory (2023). *Yellowstone Volcano Observatory 2022 Annual Report (Circular 1508)*. Circular. US Geological Survey. DOI: 10.3133/cir1508.

Zhong, S., Z. Wan, B. Duan, D. Liu, and B. Luo (2019). "Do earthquakes trigger mud volcanoes? A case study from the southern margin of the Junggar Basin, NW China". *Geological Journal* 54(3), pages 1223–1237. DOI: 10.1002/gj.3222.